Ba-Ba, K-K or Ba-K). In the present results and in the earlier work of Sabine & Hewat (1982), this shows up as an RMS static displacement contribution to the β_{33} anisotropic thermal parameters. In all the substituted hollandites, the apparent RMS amplitude of vibration U_{33} along the tunnels [given by $(\beta_{33}c^2/2\pi^2)^{1/2}$] is between two and three times the RMS amplitude U_{11} or U_{22} [given by $(\beta_{11}c^2/2\pi^2)^{1/2}$] perpendicular to the tunnel axis. In the Ba(1·24) hollandite, $U_{11} \simeq U_{33}$ and U_{11} is comparable with the values in the substituted specimens. On the assumption that the thermal vibrations are approximately isotropic and the U_{11} values are predominantly thermal in nature, an estimate of the RMS static displacement U_s will be given by $U_{33}^2 = U_{11}^2 + U_s^2$. Interpreted in this way individual off-centre shifts in the K and Rb hollandites can be anywhere between 0·15 and 0·65 Å. In the Cs-substituted hollandite the shifts are between 0·10 and 0·40 Å. The extent to which positional disorder contributes to U_{33} and U_{11} is currently under investigation.

I wish to acknowledge the support given to this work by the Australian Atomic Energy Commission (Research Contract No. 82/X/1) and the Australian Institute of Nuclear Science & Engineering.

References

BAYER, G. & HOFFMANN, W. (1966). *Am. Mineral.* **51**, 511-516.
BEYELER, H. U. (1976). *Phys. Rev. Lett.* **37**, 1557-1560.
BURSILL, L. A. & GRZINIC, G. (1980). *Acta Cryst.* B**36**, 2902-2913.
CHEARY, R. W. (1986). *Acta Cryst.* B**42**, 229-236.
CHEARY, R. W. & KWIATKOWSKA, J. (1984). *J. Nucl. Mater.* **125**, 236-243.
HOWARD, C. J. (1982). *J. Appl. Cryst.* **15**, 615-620.
HOWARD, C. J., BALL, C. J., DAVIS, L. D. & ELCOMBE, M. M. (1983). *Aust. J. Phys.* **35**, 507-518.
KESSON, S. (1983). *Radioact. Waste Manage.* **4**, 53-72.
KESSON, S. & WHITE, T. J. (1986). *Proc. R. Soc. London Ser. A.* In the press.
POST, J. E., VON DREELE, R. B. & BUSECK, P. R. (1982). *Acta Cryst.* B**38**, 1056-1065.
PRING, A. (1983). PhD Thesis, Univ. of Cambridge.
RIETVELD, H. M. (1969). *J. Appl. Cryst.* **2**, 65-71.
RINGWOOD, A. E. (1978). *Safe Disposal of High Level Radioactive Waste: A New Strategy.* Canberra: Australian National University Press.
ROTH, R. (1981). Annual Report. National Measurement Laboratory, Office for Nuclear Technology. NBSIR 81-2241.
SABINE, T. M. & HEWAT, A. W. (1982). *J. Nucl. Mater.* **110**, 173-177.
SHANNON, R. D. (1976). *Acta Cryst.* A**32**, 751-767.
SINCLAIR, W., MCLAUGHLIN, G. M. & RINGWOOD, A. E. (1980). *Acta Cryst.* B**36**, 2913-2918.
SOLOMAH, A. G. & ODOJ, R. (1984). *J. Am. Ceram. Soc.* **67**, C-50-C-51.
WEBER, H. & SCHULZ, H. (1983). *Solid State Ionics*, **9** & **10**, 1337-1340.
WILES, D. B. & YOUNG, R. A. (1981). *J. Appl. Cryst.* **14**, 149-150.

Acta Cryst. (1987). B**43**, 34-40

$Mg_7Ga_2GeO_{12}$, a New Spinelloid-Related Compound, and the Structural Relations Between Spinelloids (Including Spinel) and the β-Ga_2O_3 and NaCl Types

BY J. BARBIER

Department of Geology, University of Western Ontario, London, Ontario N6A 5B7, Canada

AND B. G. HYDE

Research School of Chemistry, Australian National University, GPO Box 4, Canberra-ACT 2601, Australia

(*Received* 25 *April* 1986; *accepted* 13 *July* 1986)

Abstract

A new compound, $Mg_7Ga_2GeO_{12}$, has been identified in the MgO–Ga_2O_3–GeO_2 system (at 1 atmosphere pressure). Its unit cell is orthorhombic with parameters $a = 5{\cdot}8493\,(5)$, $b = 25{\cdot}449\,(3)$ and $c = 2{\cdot}9816\,(3)$ Å, with $V = 443{\cdot}8$ Å^3, $Z = 2$, $D_x = 4{\cdot}30$ g cm^{-3} and $M_r = 574{\cdot}2$. A structural model, determined from powder X-ray diffraction data, shows that it is isostructural with Fe_9PO_{12}. Its crystal structure is simply related to that of the spinelloid phases and, like them, can be described as an intergrowth of the rock salt and β-Ga_2O_3 types.

1. Introduction

We recently reported the identification of a new compound, $Mg_3Ga_2GeO_8$(III) (Barbier & Hyde, 1986), stable at atmospheric pressure in the MgO–Ga_2O_3–GeO_2 system and isostructural with the spinelloid β-phase [*e.g.* β-Co_2SiO_4 (Morimoto, Tokonami, Watanabe & Koto, 1974) and $Ni_3Al_2SiO_8$(III) (Ma & Sahl, 1975)]. $Mg_3Ga_2GeO_8$(III) was the first (pseudo)ternary phase identified in that system, while the previously known (pseudo)binary phases – in the magnesium-rich region of the phase diagram – included $MgGa_2O_4$ spinel (*e.g.* Schmalzried, 1961),

0108-7681/87/010034-07$01.50

Mg_2GeO_4 olivine (*e.g.* Dachille & Roy, 1960) and $Mg_{14}Ge_5O_{24}$ (Von Dreele, Bless, Kostiner & Hughes, 1970) (Fig. 1). The present paper reports the identification and characterization of another (pseudo)-ternary compound, $Mg_7Ga_2GeO_{12}$, stable at atmospheric pressure in the MgO–Ga_2O_3–GeO_2 system.

2. Experimental

Syntheses were carried out by high-temperature sintering of constituent oxide powders: appropriate amounts of high-purity (99·99% or better) MgO, Ga_2O_3 and GeO_2 were mixed, pressed into pellets and allowed to react at 1373 K in air for two days with intermediate re-mixing operation. Portions of the product were then sealed in Pt tubes, annealed at 1673 K for two days, and finally quenched in air. (The use of sealed Pt capsules was necessary in order to prevent loss of GeO_2 vapour.)

The nature of the reaction products was checked by powder X-ray diffraction with a Guinier–Hägg focusing camera using monochromatized Cu radiation [$\lambda(K\alpha_1) = 1{\cdot}5406$ Å]. Silicon ($a = 5{\cdot}4305$ Å) was used as an internal standard; $5 \le 2\theta \le 80°$; rotating sample. Unit-cell parameters were refined by means of local least-squares refinement programs.

Some samples were also examined by electron diffraction and high-resolution electron microscopy using a JEOL 200CX electron microscope. For this purpose, a finely ground powder was dispersed in 1-butanol and deposited on a holey carbon film supported by a copper grid.

3. Results

The new compound was first recognized in reaction products from the slow decomposition of $Mg_3Ga_2GeO_8$(III) (through evaporation of GeO_2) when heated in air at 1673 K. In order to locate its exact composition, several samples with bulk compositions in the MgO–$MgGa_2O_4$–Mg_2GeO_4 triangle were prepared which yielded various mixtures of the phases shown in Fig. 1. One sample with nominal composition $7MgO.Ga_2O_3.GeO_2$ yielded a single-phase product, the powder X-ray diffraction pattern of which is given in Table 1.* With the help of an automatic indexing program (Visser, 1969), this pattern could be successfully indexed on a C-centred orthorhombic unit cell with the parameters $a = 5{\cdot}8493\ (5)$, $b = 25{\cdot}449\ (3)$, $c = 2{\cdot}9816\ (3)$ Å and $Z = 2$ (for the ideal composition $Mg_7Ga_2GeO_{12}$). The systematic extinctions, hkl, $h + k \neq 2n$, lead to three possible space groups, $Cmm2$, $C222$ and $Cmmm$, among which the last one only is centrosymmetric.

The symmetry and approximate cell dimensions were confirmed by electron diffraction from microscopic single crystals: Fig. 2 shows the [001] and [100] zone-axis electron diffraction patterns with the hkl, $h + k \neq 2n$ reflections missing.

At this stage a structural model (Figs. 3 and 4) was developed for $Mg_7Ga_2GeO_{12}$, based on the following considerations:

(*a*) The composition lies on the MgO–$Mg_2Ga_3GeO_8$ join in the MgO–Ga_2O_3–GeO_2 phase diagram (*cf.* Fig. 1), suggesting that the new compound might result from intergrowth of the two end-members.

(*b*) The unit-cell parameters are simply related to those of the β-phase $Mg_3Ga_2GeO_8$(III), *i.e.* $a \simeq a_\beta$, $b \simeq 3c_\beta$ and $c \simeq b_\beta/4$, indicating that the new structure is also based on an approximate cubic eutaxy of O atoms, with metal atoms in octahedral and tetrahedral coordination.

The validity of this model was checked by calculating the intensities of the X-ray powder diffraction lines of the model structure [using the program *LAZY-PULVERIX* (Yvon, Jeitschko & Parthé, 1977)] for comparison with the observed intensities. The calculations were carried out with a perfect c.c.p. oxygen array and atoms in the following positions of the *Cmmm* space group:

Octahedral sites 7Mg + Ga	$M(1)$	$2(a)$	0	0	0
	$M(2)$	$2(b)$	$\frac{1}{2}$	0	0
	$M(3)$	$4(i)$	0	$\frac{1}{6}$	0
	$M(4)$	$8(q)$	$\frac{1}{4}$	$\frac{1}{12}$	$\frac{1}{2}$
Tetrahedral sites Ga + Ge	T	$4(j)$	0	$\frac{7}{24}$	$\frac{1}{2}$
	O(1)	$4(h)$	$\frac{1}{4}$	0	$\frac{1}{2}$
	O(2)	$4(i)$	0	$\frac{1}{12}$	0
	O(3)	$4(i)$	0	$\frac{3}{4}$	0
	O(4)	$4(i)$	0	$\frac{5}{12}$	0
	O(5)	$8(q)$	$\frac{1}{4}$	$\frac{1}{6}$	$\frac{1}{2}$

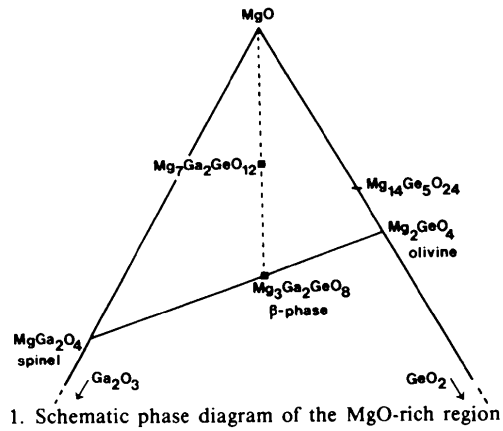

Fig. 1. Schematic phase diagram of the MgO-rich region of the MgO–Ga_2O_3–GeO_2 system at atmospheric pressure and 1673 K. Two (pseudo)ternary phases have been identified: $Mg_3Ga_2GeO_8$(III) with the β-phase structure (Barbier & Hyde, 1986) and $Mg_7Ga_2GeO_{12}$ (this work).

* Powder diffraction data have been deposited with the British Library Document Supply Centre as Supplementary Publication No. SUP 43225 (2 pp.). Copies may be obtained through The Executive Secretary, International Union of Crystallography, 5 Abbey Square, Chester CH1 2HU, England.

Table 1. *Powder X-ray diffraction pattern of* $Mg_7Ga_2GeO_{12}$

All calculated lines have been included in the range $0 \leq 2\theta \leq 64°$. 21 unobserved lines with calculated intensities less than 1% have been omitted in the range $64 \leq 2\theta \leq 80°$.

2θ(°)	I/I_o	I_{calc}	d_{exp}(Å)	d_{calc}(Å)	h	k	l	$\Delta 2\theta$*(°)
—	—	8	—	12·72	0	2	0	—
13·88	4	5	6·37	6·36	0	4	0	−0·028
15·50	5	0·1	5·71	5·70	1	1	0	−0·029
18·38	3	5	4·823	4·815	1	3	0	−0·030
—	—	0		4·241	0	6	0	—
23·14	35	23	3·841	3·840	1	5	0	−0·010
28·02	8	7	3·182	3·181	0	8	0	−0·008
28·89	20	34	3·088	3·088	1	7	0	−0·003
29·93	15	11	2·9827	2·9816	0	0	1	−0·012
30·54	13	10	2·9248	2·9246	2	0	0	−0·001
30·77	15	8	2·9030	2·9030	0	2	1	−0·001
31·35	20	23	2·8512	2·8503	2	2	0	−0·010
33·15	3	0·5	2·7000	2·6998	0	4	1	−0·002
33·70	35	22	2·6576	2·6573	2	4	0	−0·003
—	—	7	—	2·6420	1	1	1	—
35·22	62	19	2·5460	2·5458	1	9	0	−0·003
		17		2·5449	0	10	0	−0·016
35·38		37	2·5352	2·5350	1	3	1	−0·003
37·27	5	2	2·4108	2·4077	2	6	0	−0·048
38·18	26	32	2·3553	2·3549	1	5	1	−0·006
41·50	13	12	2·1740	2·1754	0	8	1	0·028
—	—	0·2	—	2·1530	2	8	0	—
—	—	2	—	2·1513	1	11	0	—
42·11	18	9	2·1443	2·1448	1	7	1	0·011
42·59	18	19	2·1209	2·1207	0	12	0	−0·004
43·30	46	35	2·0880	2·0879	2	0	1	−0·003
43·91	44	35	2·0603	2·0603	2	2	1	0·001
45·70	4	7	1·9835	1·9834	2	4	1	0·007
—	—	0	—	1·9440	3	1	0	—
—	—	0·8	—	1·9361	1	9	1	—
46·91	7	7	1·9354	1·9357	0	10	1	0·008
—	—	2	—	1·9198	2	10	0	—
—	—	0·4	—	1·9002	3	3	0	—
—	—	0	—	1·8732	2	6	1	—
—	—	1	—	1·8564	1	13	0	—
50·07	12	3	1·8204	1·8207	3	5	0	0·009
—	—	6		1·8178	0	14	0	—
52·39	5	0·7	1·7451	1·7455	2	8	1	0·014
		0		1·7446	1	11	1	−0·014
52·94	6	4	1·7283	1·7282	0	12	1	−0·003
53·30	11	6	1·7174	1·7183	3	7	0	0·028
		4		1·7169	2	12	0	−0·019
56·43	6	5	1·6294	1·6294	1	15	0	0·002
		2		1·6285	3	1	1	−0·034
—	—	0·3	—	1·6142	2	10	1	—
—	—	4	—	1·6052	3	9	0	—
57·46	22	9	1·6024	1·6024	3	3	1	0·001
—	—	0·8	—	1·5906	0	16	0	—
58·53	7	0	1·5758	1·5759	1	13	1	0·005
59·43	10	8	1·5539	1·5539	3	5	1	0·000
—	—	3	—	1·5521	0	14	1	—
—	—	1	—	1·5439	2	14	0	—
—	—	0·6	—	1·4909	3	11	0	—
62·22	100	19	1·4908	1·4908	0	0	2	0·001
—		3	—	1·4887	3	7	1	—
62·74		78	1·4877	1·4878	2	12	1	0·007
—	—	0	—	1·4807	0	2	2	—
63·57	27	18	1·4623	1·4623	4	0	0	0·001
64·18	3	3	1·4499	1·4502	1	17	0	0·016
66·59	6	3	1·4032	1·4033	0	16	1	0·010
66·93	6	0	1·3970	1·3973	2	16	0	0·015
67·31	4	2	1·3899	1·3897	1	5	2	−0·008
70·01	3	5	1·3427	1·3425	1	7	2	−0·013
70·88	4	1	1·3285	1·3287	4	8	0	0·008
		2		1·3282	2	0	2	−0·020
71·35	3	4	1·3208	1·3210	2	2	2	0·012
71·84	2	2	1·3130	1·3129	4	0	1	−0.003
72·35	5	1	1·3050	1·3056	1	19	0	0·037
		2		1·3042	1	17	1	−0·056
72·67	11	4	1·3000	1·3002	2	4	2	0·007
73·61	14	4	1·2858	1·2864	1	9	2	0·044
		4		1·2863	0	10	2	0·036
		0·1		1·2858	4	4	1	0·003
74·01	5	2	1·2798	1·2799	3	15	0	0·003
74·13	5	1	1·2780	1·2775	0	18	1	−0·034
74·83	13	3	1·2677	1·2679	4	10	0	0·011
		2		1·2675	2	6	2	−0·017
75·83	3	1	1·2536	1·2542	4	6	1	0·043

Table 1 (*cont.*)

2θ(°)	I/I_o	I_{calc}	d_{exp}(Å)	d_{calc}(Å)	h	k	l	$\Delta 2\theta$*(°)
78·34	4	4	1·2195	1·2196	0	12	2	0·007
78·79	3	3	1·2137	1·2136	4	8	1	−0·007
79·58	6	4	1·2037	1·2039	4	12	0	0·016

* $\Delta 2\theta = 2\theta_{exp} - 2\theta_{calc}$.

This set of atomic coordinates and cation distributions resulted in a satisfactory agreement between observed and calculated intensities (*cf.* Table 1; the reliability factor $R = \sum|I_o - I_c|/\sum I_o = 0{\cdot}33$), thus supporting the structural model proposed.

Additional information consistent with this model was provided by electron diffraction and high-reso-

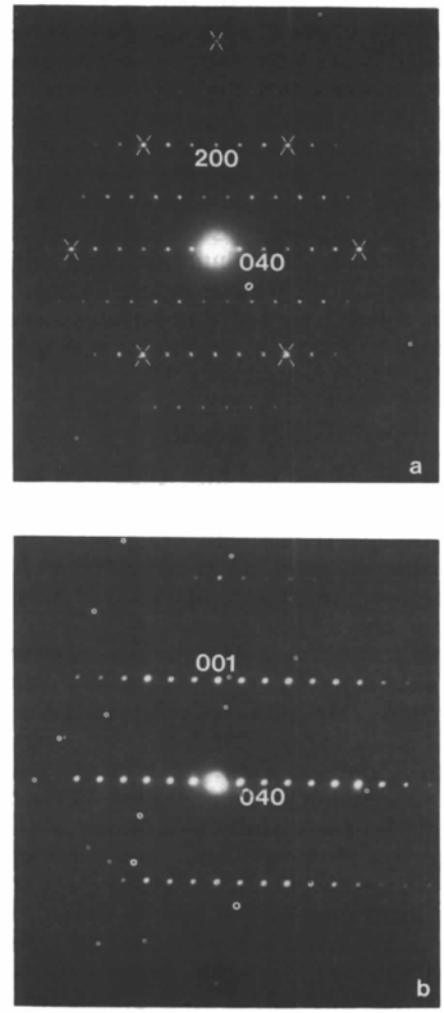

Fig. 2. (*a*) [001] and (*b*) [100] zone-axis electron diffraction patterns of $Mg_7Ga_2GeO_{12}$. Note the absence of the *hkl*, $h + k \neq 2n$ reflections consistent with the *C*-centred unit cell. Reflections corresponding to the [110] zone of the MgO unit cell have been emphasized in (*a*).

lution electron microscopy. [001] zone-axis electron diffraction patterns (*cf.* Fig. 2 and the diffraction pattern in Fig. 5) showed intense substructure reflections corresponding to a [110] zone-axis diffraction pattern of the face-centred cubic MgO unit cell with the orientation relationships $[001]_{sub}\|[010]$ and $[\bar{1}10]_{sub}\|[100]$. This observation is consistent with the proposed $Mg_7Ga_2GeO_{12}$ structure depicted in Figs. 3 and 4, containing large blocks with the rock-salt structure.

A high -resolution image of an $Mg_7Ga_2GeO_{12}$ crystal viewed down the [001] zone axis (Fig. 5) shows double rows of bright dots parallel to the **a** axis. By comparison with the drawing of the [001] projection of the structure (Fig. 3), these dots can be associated with the projected positions of the [001] rows of corner-sharing $(Ga,Ge)O_4$ tetrahedra.

High-resolution imaging also revealed a number of faulted crystals, the faults being perpendicular to the **b** direction (Fig. 6). This is again consistent with the $Mg_7Ga_2GeO_{12}$ structure being built up of blocks stacked in the **b** direction. However, no significant intergrowths nor highly disordered crystals were

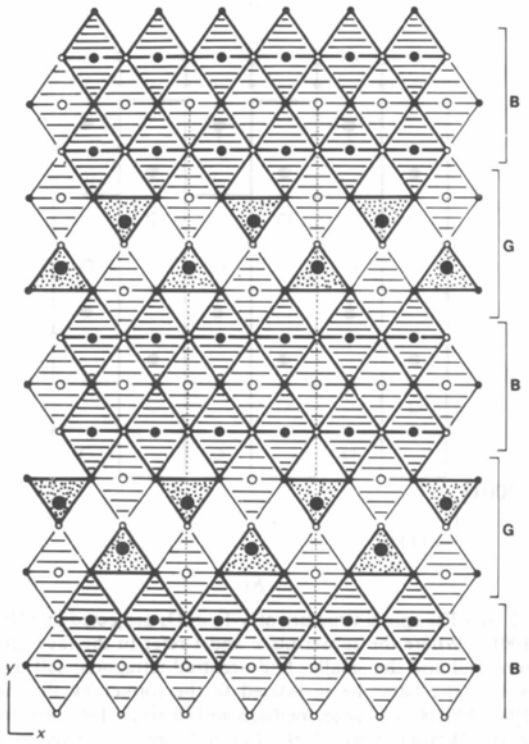

Fig. 3. The ideal $Mg_7Ga_2GeO_{12}$ structure projected on (001), consisting of blocks with the rock-salt (B) and β-Ga_2O_3 (G) structures alternating in the y direction. Large, medium and small circles are (Ga,Ge), (Mg,Ga) and O atoms respectively. Open and filled circles are at heights 0 and 50 (in units of $c/100$) respectively.

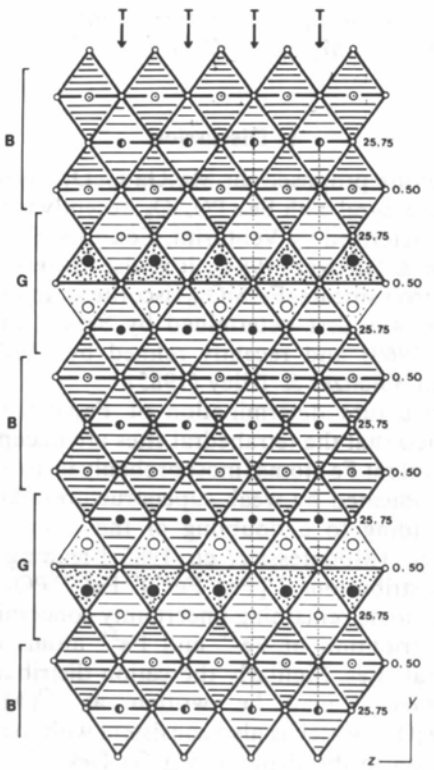

Fig. 4. The ideal $Mg_7Ga_2GeO_{12}$ structure projected on (100). (B) and (G) symbols as in Fig. 3. Note the straight [001] rows of corner-sharing tetrahedra generated by the T boundaries. Large, medium and small circles are (Ga,Ge), (Mg,Ga) and O atoms respectively. Open, filled and dotted circles (cations only) are at heights 0, 50 and ±25 (in units of $a/100$) respectively (half-filled circles are at heights 0 and 50). The heights of O atoms are given in units of $a/100$.

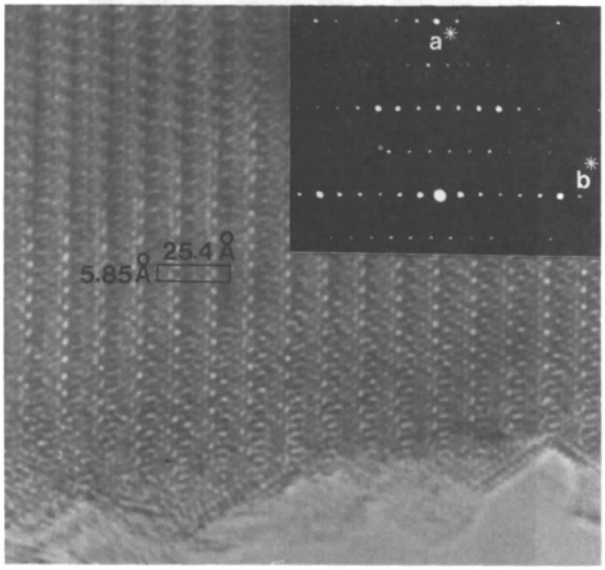

Fig. 5. High-resolution image of a $Mg_7Ga_2GeO_{12}$ crystal viewed down the [001] zone-axis. The double rows of bright dots are associated with the projected positions of the [001] rows of $(Ga,Ge)O_4$ tetrahedra (*cf.* Fig. 3). One unit cell has been outlined.

observed in multiphase samples containing MgO, $Mg_7Ga_2GeO_{12}$, $Mg_3Ga_2GeO_8$(III) and $MgGa_2O_4$.

4. Discussion

The structure proposed for $Mg_7Ga_2GeO_{12}$ shows that it is isostructural with $Fe_9(PO_4)O_8$, recently identified and characterized by Venturini, Courtois, Steinmetz, Gerardin & Gleitzer (1984). It is also closely related to a rare iron silicate, Fe_7SiO_{10} (iscorite), the structure of which was first determined by Smuts, Steyn & Boyers (1969) and recently refined by Modaressi, Malaman, Gleitzer & Tilley (1985).

The structure determination of $Fe_9(PO_4)O_8$ has established that the tetrahedral sites are occupied by P and divalent Fe atoms [most probably in an ordered way as indicated by weak superstructure reflections corresponding to a doubling of the a and c cell parameters (Modaressi *et al.*, 1985)] leading to the cation distributions $^{VI}[Fe_7^{2+}Fe^{3+}]^{IV}Fe^{2+IV}PO_{12}$ with, however, some remaining uncertainty concerning the exact distribution of Fe^{2+} and Fe^{3+} atoms on the octahedral sites. Similarly the cation distribution in $Mg_7Ga_2GeO_{12}$ may be written as $^{VI}[Mg_7Ga]$-$^{IV}[GaGe]O_{12}$, which is also consistent with the cation distribution in the β-phase $Mg_3Ga_2GeO_8$(III) (Barbier & Hyde, 1986). Electron diffraction did not reveal any superstructure, which indicates that the Ga and Ge atoms are disordered on the tetrahedral sites.

Although the $Fe_9(PO_4)O_8$ and $Mg_7Ga_2GeO_{12}$ crystal structures correspond to a new structure type, we show below that they are very simply related to well-known structures such as spinel (and the spinelloids) and β-Ga_2O_3.

As described by Hyde, White, O'Keeffe & Johnson (1982), the spinel structure (Fig. 7*a*) is built up of identical blocks, stacked in the [110] direction and related by antiphase boundaries (S). (These blocks are emphasized in Fig. 7*b*, which shows only the

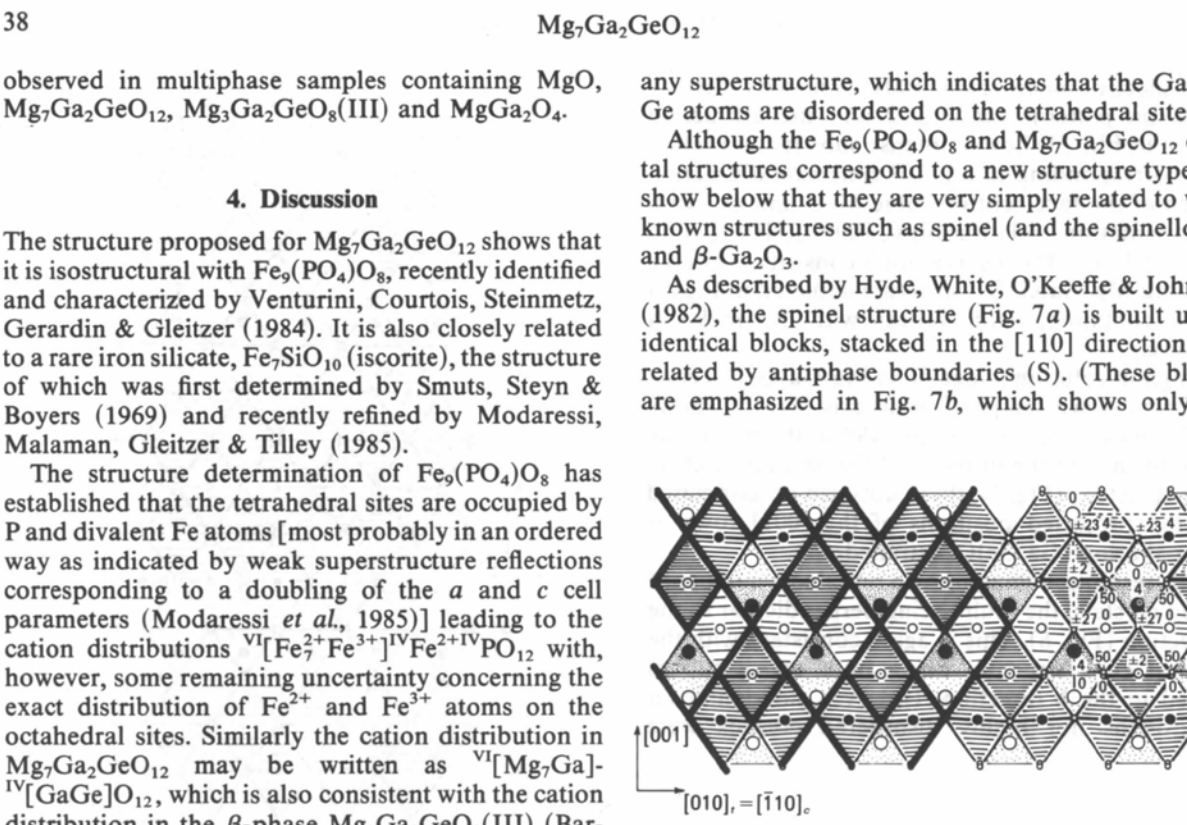

Fig. 7. (*a*) The spinel structure of γ-Fe_2SiO_4 projected on $(110)_c = (100)_t$. [Where the subscripts c and t refer to the face-centred cubic cell and the smaller body-centred tetragonal cell respectively – the latter being related to the former by the matrix $(\frac{1}{2}\frac{1}{2}0/-\frac{1}{2}\frac{1}{2}0/001)$.] Large, medium and small circles represent Si, Fe and O atoms respectively. Cation heights are given in units of $a_t/8$ and anion heights in units of $a_t/100$. The left-hand part of the figure emphasizes the intergrowth of β-Ga_2O_3 elements (V-shaped columns) and rock-salt elements (single octahedral columns). (*b*) As (*a*) but with anions omitted. The elementary building blocks of the spinel and spinelloid structures have been emphasized. Adjacent slabs are related by antiphase boundaries (S).

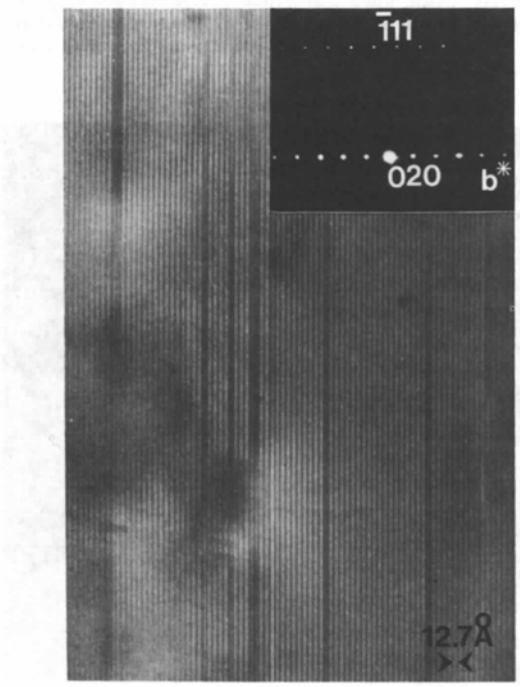

Fig. 6. Faulted $Mg_7Ga_2GeO_{12}$ crystal seen along the [101] direction. Faults such as these, perpendicular to the y direction, might correspond to 'errors' in the thickness of the rock-salt or β-Ga_2O_3 blocks in the $Mg_7Ga_2GeO_{12}$ structure.

cations. The displacement vector between adjacent slabs is $\mathbf{R} = \mathbf{a}[112]/4$, which leaves the oxygen array invariant to a first approximation.) The same blocks are readily recognized in the [100] projection of the $Mg_7Ga_2GeO_{12}$ structure (Fig. 4), alternating with elements of the rock-salt structure along the **b** direction. In this case, however, they repeat by simple translation parallel to the **c** axis so that all the S boundaries of the spinel structure have been replaced by pseudo-mirror planes [or T (twin) boundaries in the notation of Hyde *et al.* (1982)]. This generates straight rows of corner-sharing TO_4 tetrahedra, and an identical rod unit is encountered in the structure of the hypothetical end-member of the spinelloid family, the so-called Ω-phase depicted in Fig. 8. [Indeed the Ω-phase structure is generated from the spinel structure – the other end-member of the spinelloid series – by the same operation as described above, *i.e.* the transformation of all S boundaries into T boundaries (Hyde *et al.*, 1982).] It follows that, as illustrated by Figs. 4 and 8, the $Mg_7Ga_2GeO_{12}$ structure can be regarded as an intergrowth of the Ω-phase and rock-salt structures along [010], which can be formulated as follows:

$$Mg_7Ga_2GeO_{12} = 4\ MgO\ \text{(rock salt)} + Mg_3Ga_2GeO_8\ (\Omega\text{-phase})$$

Referring to the MgO–$Mg_3Ga_2GeO_8$(III) join in the phase diagram (Fig. 1) it then appears that intergrowth of the two end-members promotes the transformation from the spinelloid β-phase into the spinelloid Ω-phase. The latter has been proposed as the first step in a martensitic-type mechanism for the high-pressure olivine → spinel transformation (Hyde *et al.*, 1982) and, to our knowledge, $Mg_7Ga_2GeO_{12}$ is the first example of an oxide in which the Ω-phase is recognized as such. [Ω-phase blocks also occur in the Fe_7SiO_{10} (iscorite) structure but are, in this case, intergrown with two rock-salt (FeO) blocks of different sizes, leading to a monoclinic unit cell.]

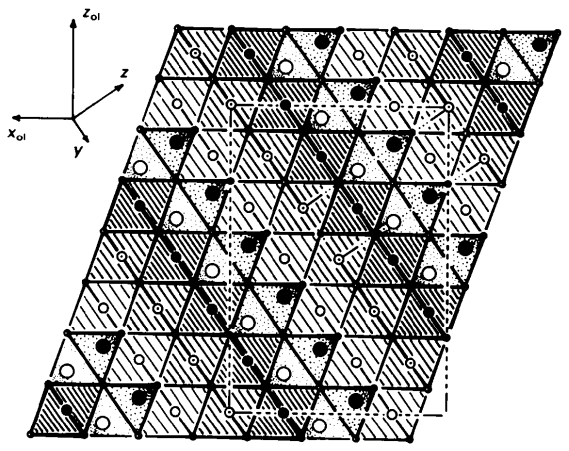

Fig. 8. The structure of the hypothetical spinelloid Ω-phase projected on (100) (after Hyde *et al.*, 1982). The relation to the $Mg_7Ga_7GeO_{12}$ structure (Fig. 4) is obvious: the only difference lies in the thickness of the rock-salt layer alternating with β-Ga_2O_3 elements. [The larger olivine-related unit cell illustrates the fact that the Ω-phase structure corresponds to a cubic stacking of (001) olivine layers (Hyde *et al.*, 1982).]

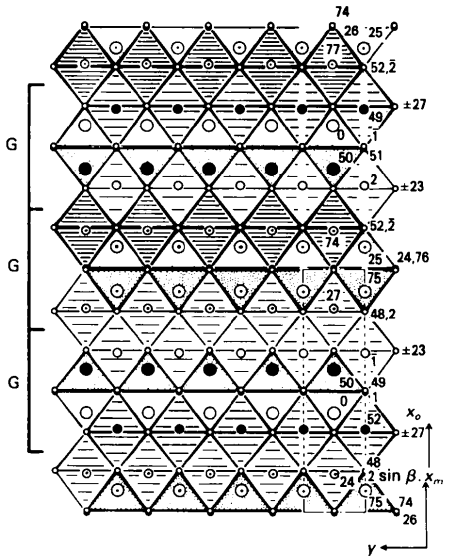

(*a*)

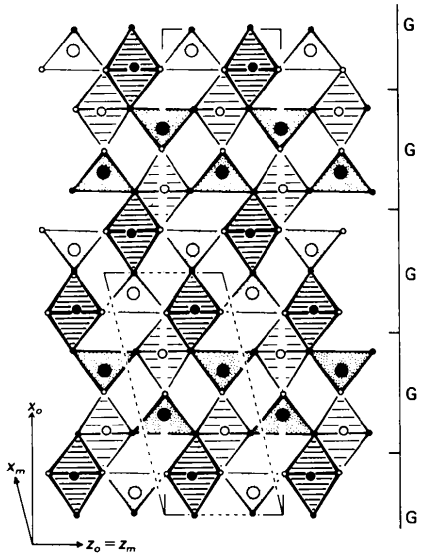

(*b*)

Fig. 9. (*a*) The β-Ga_2O_3 structure projected along $z_m = z_o$. (The subscripts *m* and *o* refer to the true monoclinic and equivalent orthorhombic unit cells respectively – *cf.* Fig. 9*b*.) Large and medium circles are Ga atoms in tetrahedral and octahedral coordination respectively. Small circles are O atoms. Heights are given in units of *c*/100. Compare with Figs. 4 and 8. (*b*) The β-Ga_2O_3 structure projected on (010). Both the monoclinic and equivalent orthorhombic unit cells have been outlined. Large and medium circles are Ga atoms and small circles are O atoms. Open and filled circles are at heights 0 and 50 (in units of *b*/100). Compare with Figs. 3 and 10.

The infinite rows of corner-sharing tetrahedra present in the $Mg_7Ga_2GeO_{12}$ and Ω-phase structures are also found in the β-Ga_2O_3 structure, parallel to the **b** direction (Fig. 9*a*).* In $Mg_7Ga_2GeO_{12}$ the β-Ga_2O_3 blocks (denoted G in Figs. 3 and 4) have the stoichiometry $MgGa_2GeO_6 = {}^{VI}(MgGa)^{IV}(GaGe)O_6$ and alternate in the y direction with rock-salt blocks (denoted B for B1) with the stoichiometry Mg_6O_6. Accordingly the $Mg_7Ga_2GeO_{12}$ structure can be described as an intergrowth of the β-Ga_2O_3 and rock-salt structure types, which is best recognized by comparing Figs. 3 and 9(*b*) (*i.e.* the short-axis projections for both structures).

The Ω-phase can similarly be regarded as an intergrowth of the β-Ga_2O_3 and rock-salt structures, which can be formulated as $A_2B_4O_8 = 2BO$ (rock salt) and $2ABO_3$ (β-Ga_2O_3),† where A and B are tetrahedral and octahedral cations respectively. Because the Ω-phase and spinel structures are built of the same blocks (*cf.* above), it follows that the spinel structure itself can also be described as an intergrowth of the rock-salt and β-Ga_2O_3 structure types. This is illustrated in Fig. 10 showing the $[100]_t = [110]_c$ projection of a single spinel block: once again, rock-salt (B) and β-Ga_2O_3 (G) elements alternate in the z direction, and the relation to the β-Ga_2O_3 structure (Fig. 9*b*) is obvious. Consequently the spinel structure, as a whole, consists of alternating columns of MgO and β-Ga_2O_3 types (or columns of MgO in a β-Ga_2O_3 matrix) (*cf.* left-hand side of Fig. 7*a*).

The easy intergrowth of these two structures could explain the rather strange behaviour in the high-temperature region of the phase diagrams of systems such as NiO–Al_2O_3, MgO–Al_2O_3 and MgO–Ga_2O_3. In all cases the solubility of Al_2O_3 (Ga_2O_3) in spinel is enormous, *e.g.* up to ~84% Al_2O_3/16% $MgAl_2O_4$ at 2193 K. Recalling that one modification of alumina, θ-Al_2O_3, has the β-Ga_2O_3 structure, it appears that the solubility is simply due to an increase in the ratio of β-Ga_2O_3/MO elements in the structure of the non-stoichiometric 'spinel' phase. As well, the various high-temperature metastable phases widely reported in these systems (*e.g.* Bassoul, Lefebvre & Gilles, 1974) are likely to result from ordered intergrowths of the β-Ga_2O_3 and rock-salt compounds at high β-Ga_2O_3/MO ratios. (Note, however, that the present $Mg_7Ga_2GeO_{12}$ structure corresponds to a low β-Ga_2O_3/MO ratio.)

* And also, of course, in other structures *e.g.* sillimanite Al_2SiO_5.

† Note that the β-Ga_2O_3 structure is (crystallographically) quinquenary, with two cation sites, as well as three anion sites.

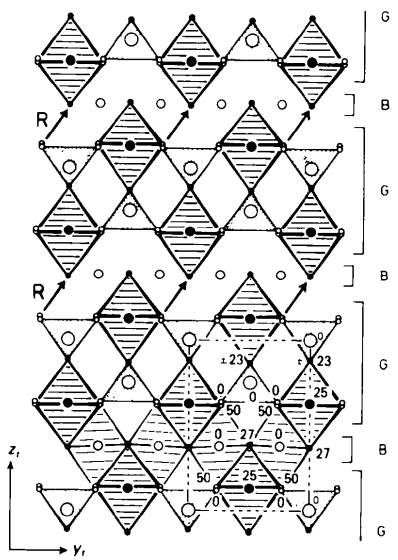

Fig. 10. The structure of a single (γ-Fe_2SiO_4) spinel block projected on $(100)_t$. Large, medium and small circles are Si, Fe and O atoms respectively. Atom heights (in units of $a_t/100$) refer to the tetragonal spinel unit cell. Arrows indicate the crystallographic shear operation needed to transform the spinel structure into the β-Ga_2O_3 structure. Compare with Fig. 9(*b*).

References

BARBIER, J. & HYDE, B. G. (1986). *Phys. Chem. Miner.* Submitted.

BASSOUL, P., LEFEBVRE, A. & GILLES, J. C. (1974). *J. Solid State Chem.* **10**, 56-65.

DACHILLE, F. & ROY, R. (1960). *Am. J. Sci.* **258**, 225-246.

HYDE, B. G., WHITE, T. J., O'KEEFFE, M. & JOHNSON, A. W. S. (1982). *Z. Kristallogr.* **160**, 53-62.

MA, C. B. & SAHL, K. (1975). *Acta Cryst.* B**31**, 2141-2143.

MODARESSI, A., MALAMAN, B., GLEITZER, C. & TILLEY, R. J. D. (1985). *J. Solid State Chem.* **60**, 107-114.

MORIMOTO, N., TOKONAMI, M., WATANABE, M. & KOTO, K. (1974). *Am. Mineral.* **59**, 475-485.

SCHMALZRIED, H. (1961). *Z. Phys. Neue Folge*, **28**, 203-219.

SMUTS, J., STEYN, J. G. D. & BOYERS, J. C. A. (1969). *Acta Cryst.* B**25**, 1251-1255.

VENTURINI, G., COURTOIS, A., STEINMETZ, J., GERARDIN, R. & GLEITZER, C. (1984). *J. Solid State Chem.* **53**, 1-12.

VISSER, J. W. (1969). *J. Appl. Cryst.* **2**, 89-95.

VON DREELE, R. B., BLESS, P. W., KOSTINER, E. & HUGHES, R. E. (1970). *J. Solid State Chem.* **2**, 612-618.

YVON, K., JEITSCHKO, W. & PARTHÉ, E. (1977). *J. Appl. Cryst.* **10**, 73-74.